Aust. J. Phys., 1987, **40**, 527–45

Observation and Analysis of Nanosecond Time-resolved R.F. Corona in Air and Comparison with N_2

N. Sato[A,B] *and S. C. Haydon*[A]

[A] Department of Physics, University of New England,
Armidale, N.S.W. 2351, Australia.
[B] Present address: Department of Electrical Engineering,
Faculty of Engineering, Hokkaido University, Sapporo 060, Japan.

Abstract

The onset of r.f. corona and the subsequent development of intermittent and continuous breakdown phenomena have been investigated in air in the space between a hyperboloidal needle-point and plane electrode for pressures from 80 to 650 Torr. Detailed records of the spatio-temporal development of the plasma and the complementary nanosecond time-resolved spectral emissions, with high spatial resolution, provide comparisons with corresponding data previously reported for nitrogen. The significant differences in the behaviour of the two gases are identified and attributed to the dominant role of electron attachment processes in the space-charge modified electric fields in air.

1. Introduction

Recent papers have reported highly time-resolved image intensified and spatially resolved spectroscopic investigations of r.f. corona between a hyperboloidal needle and plane electrodes in N_2 gas (Sato and Haydon 1986*a*, 1986*b*). Threshold voltages V_c for the critical onset of the r.f. corona were measured over a wide range of values of pd (p is the gas pressure and d the electrode separation). Further increase in the applied voltage led first to intermittent breakdown of the discharge gap at voltages V_i, prior to the establishment of a continuous spark breakdown at voltages V_{sc}.

Similar studies have now been extended to air in which the electronegative properties of oxygen would be expected to play a significant role in the development of the critical corona and the subsequent transitions to spark discharges. The same hyperboloidal needle to plane electrode configuration was used. A pulsed r.f. potential of frequency 10 MHz, pulse duration 10 μs and repetition rate of 50 Hz was applied to the plane electrode. The corona images were observed with a three-stage image intensifier system. The spectroscopic observations were made using a 0·25 mm grating monochromator, two-stage micro-channel plate (MCP) image intensifier and an optical multi-channel analyser system (OMA 2 system). The time-resolved images and spectra were obtained by using an electrical shutter in the first-stage MCP, with 10 ns exposure. The procedures used for recording both the intensified images and the ratios of the intensities of spectral lines were identical to those described in detail elsewhere (Sato and Haydon 1984*a*, 1984*b*, 1986*a*, 1986*b*).

Observations have been made at various time intervals T after the start of the applied r.f. pulse, at various phases within the individual cycles of r.f. voltage and at

0004-9506/87/040527$02.00

various peak voltage amplitudes. The value of $(V_p)_{max}$ was measured at the flat part of the r.f. pulse envelope which had a constant rise time of 2 μs.

Detailed comparisons with the results obtained in N_2 have been made over the pressure range 80 to 650 Torr (1 Torr $\equiv$ 133 Pa; temperature T = 20°C) and this paper emphasises those features which show distinctly different behaviour from the corresponding observations in nitrogen.

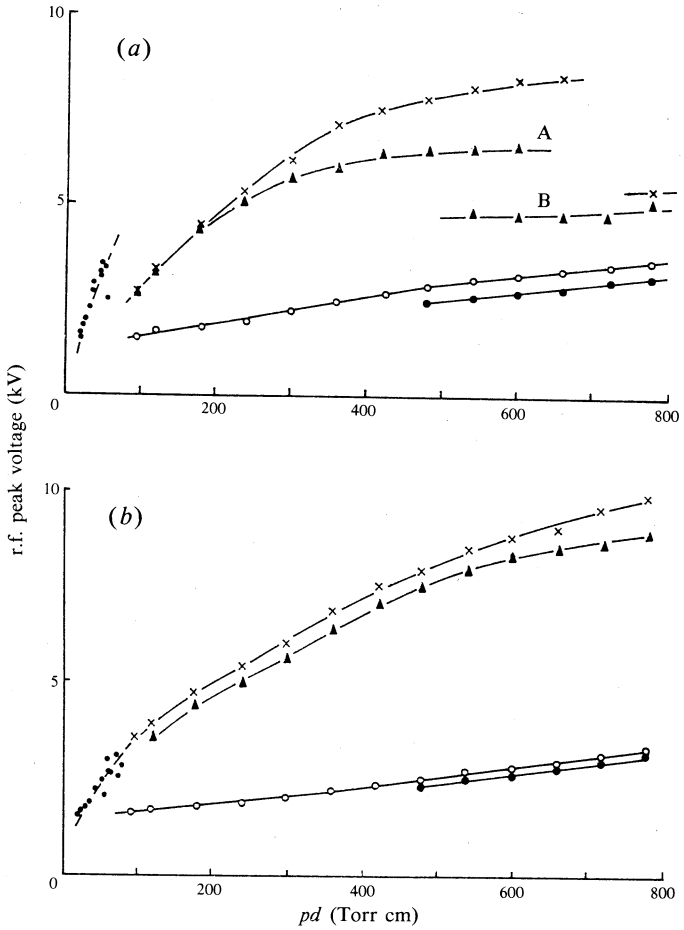

Fig. 1. Voltages V_{sc} (crosses), V_i (triangles), V_c (open circles) and V_{ext} (solid circles) against pd in (a) air and (b) nitrogen. The curves A and B are discussed in the text.

2. Experimental Results

(a) Observation of the Corona Onset

The variation of the corona onset voltage V_c with pd (d = 1·2 cm) is shown in Fig. 1a together with the corona extinction voltage V_{ext}, the intermittent breakdown voltage V_i and the continuous spark breakdown voltage V_{sc}. As in the experiments with nitrogen, the axial length of the corona discharge region d_c at the onset of corona was measured from the recorded intensified image. Recognising that the length d_c depends on the sensitivity of the optical system, we adjusted the lens aperture for the

observation in air to ensure that meaningful comparisons of the d_c values could be made. The lens aperture attached to the final stage intensifier was set to $F = 2{\cdot}8$ for air and changed from $F = 4$ to $5{\cdot}6$ for nitrogen. The lens aperture fully opened is $F = 1{\cdot}4$. The value of d_c was observed to decrease with increasing pressure. However, in air it was noted that whilst V_c increased sharply with increasing pd_c values, the V_c versus pd_c curve (dashed curve in Fig. 1*a*) did not coincide with the extrapolation of the V_{sc} versus pd curve as was the case in N_2 (Fig. 1*b*).

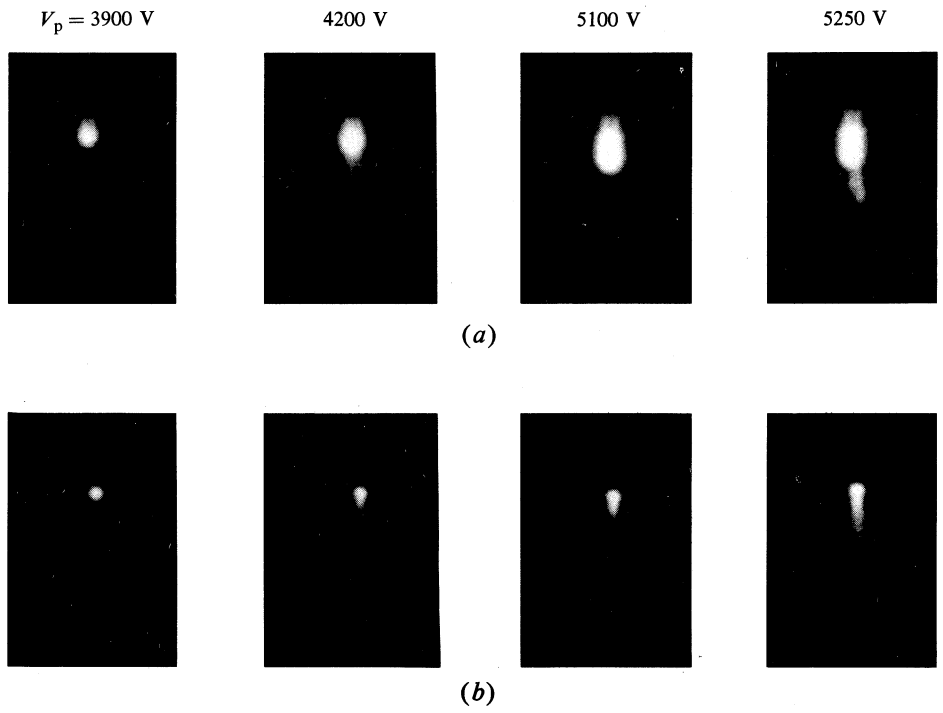

Fig. 2. Variation of the corona image with increasing r.f. voltages V_p at $T = 6$ μs and $p = 430$ Torr in air, taken at (*a*) peak positive voltage with 50 exposures and (*b*) peak negative voltage with 400 exposures.

Further significant differences were noted at values of $pd > 500$ Torr cm where, under certain conditions, the intermittent breakdown voltage V_i in air showed a marked drop from curve A to curve B. The luminous phenomena associated with these changes are clearly identified in air (see Fig. 2) through the sequence of multi-exposed corona images measured at increasing values of the applied voltage V_p.

With the needle electrode at the peak positive potential $V_p = 3900$ V, the corona discharge at 430 Torr was confined to a small volume around the needle tip. With increasing applied voltage ($V_p = 4200$ V) a filamentary luminosity extends irregularly from the surface of the corona boundary and, intermittently, may extend to the plane electrode producing the observed intermittent breakdown. Further increase in the applied voltage ($V_p = 5100$ V) leads to stabilisation of the corona discharge over a larger volume around the needle point with no evidence of filamentary extensions. A further increase in the applied voltage ($V_p = 5250$ V), however, leads to further

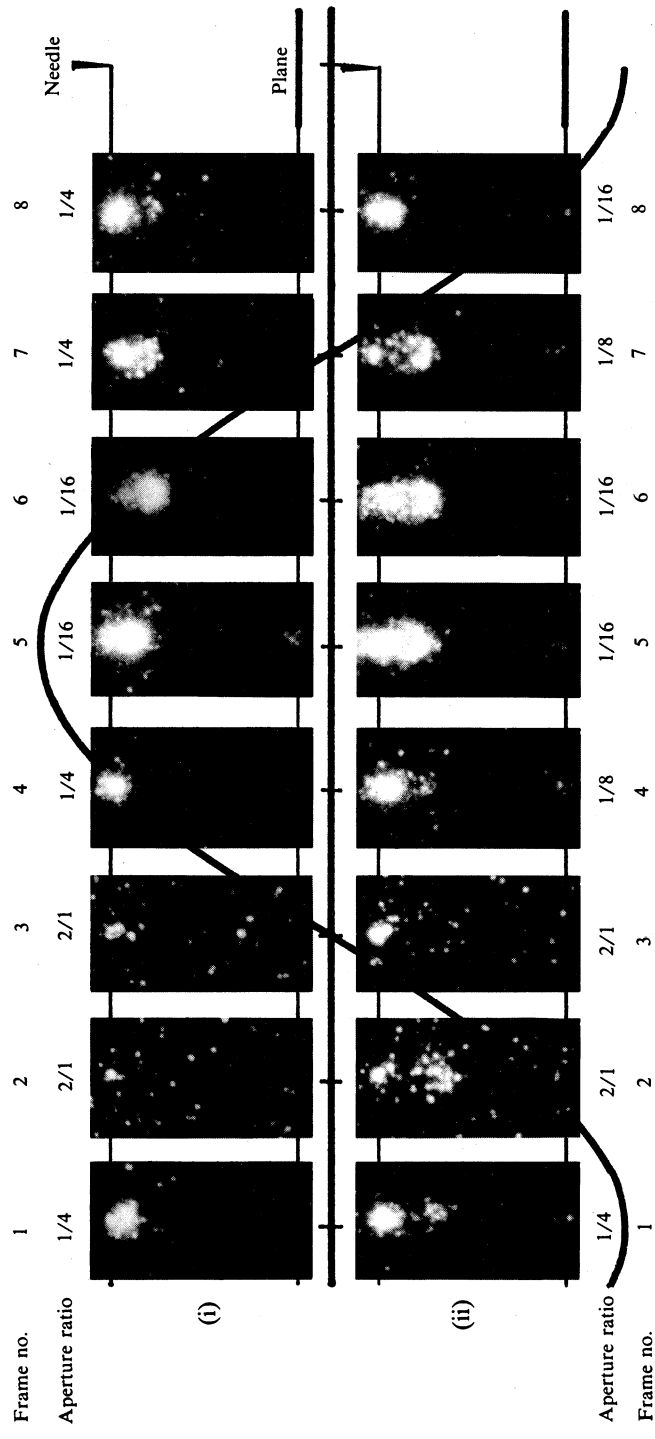

Fig. 3. Variation of the corona image at 200 Torr in air for an r.f. pulse voltage $(V_p)_{max} = 4200$ V at (i) $T = 0{\cdot}75$ μs and r.f. peak voltage $V_p = 2250$ V; (ii) $T = 0{\cdot}9$ μs and $V_p = 2550$ V; (iii) $T = 1{\cdot}4$ μs and $V_p = 3150$ V; (iv) $T = 5$ μs and $V_p = 4200$ V.

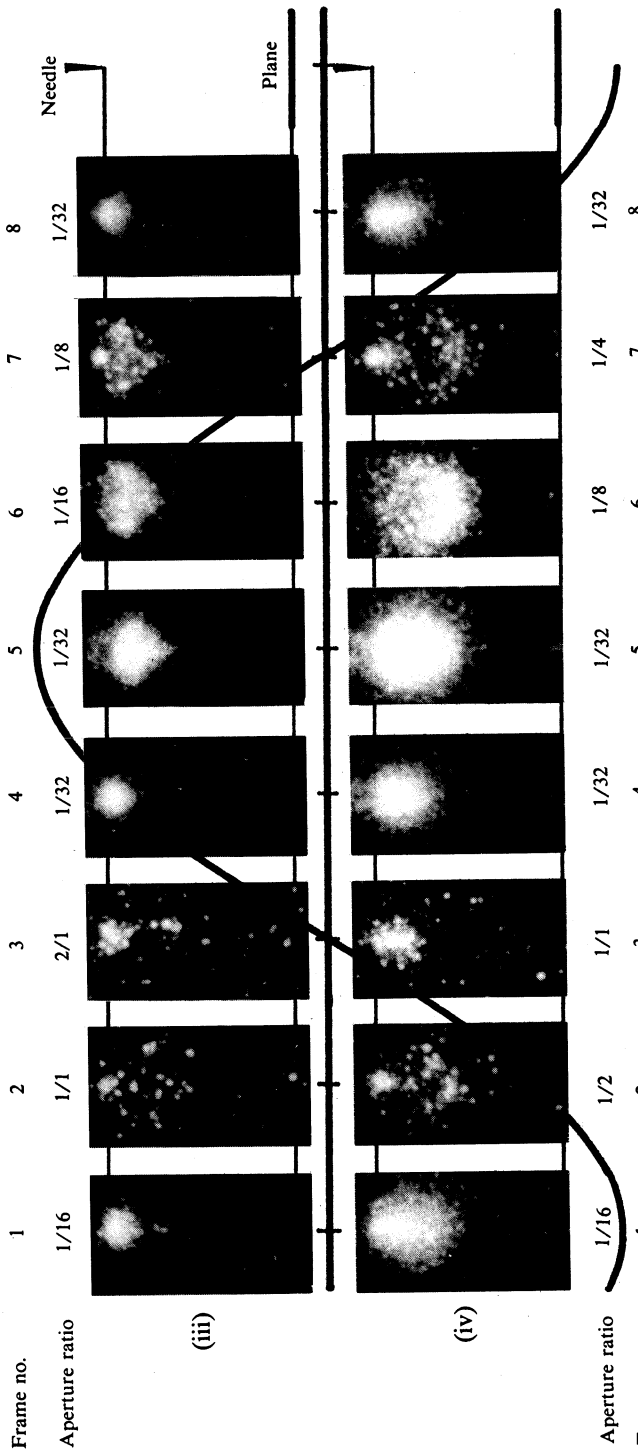

Fig. 3. (*Continued*)

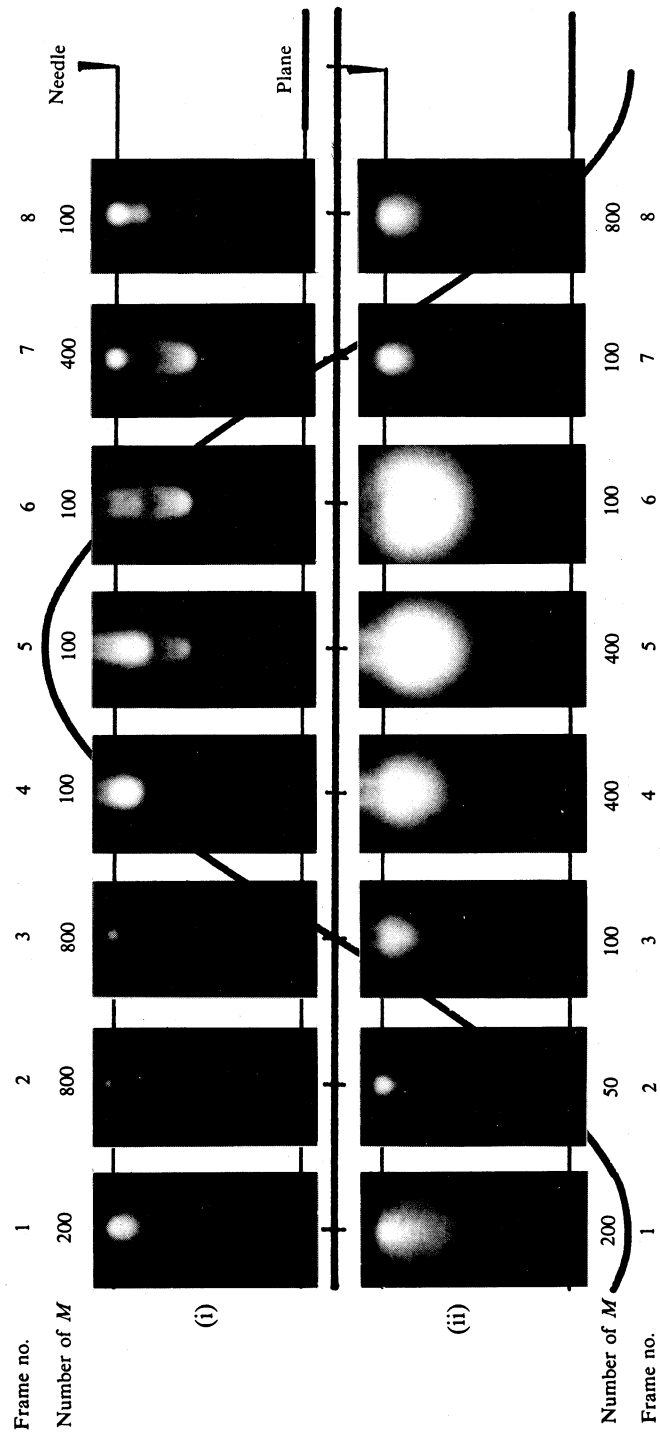

Fig. 4. Variation of the corona image at 200 Torr in air taken with two-stage MCP image intensification and multi-exposures (where M is the number of exposures) at (i) $T = 1{\cdot}0$ μs and $V_p = 2700$ V; (ii) $T = 5$ μs and $V_p = 4200$ V.

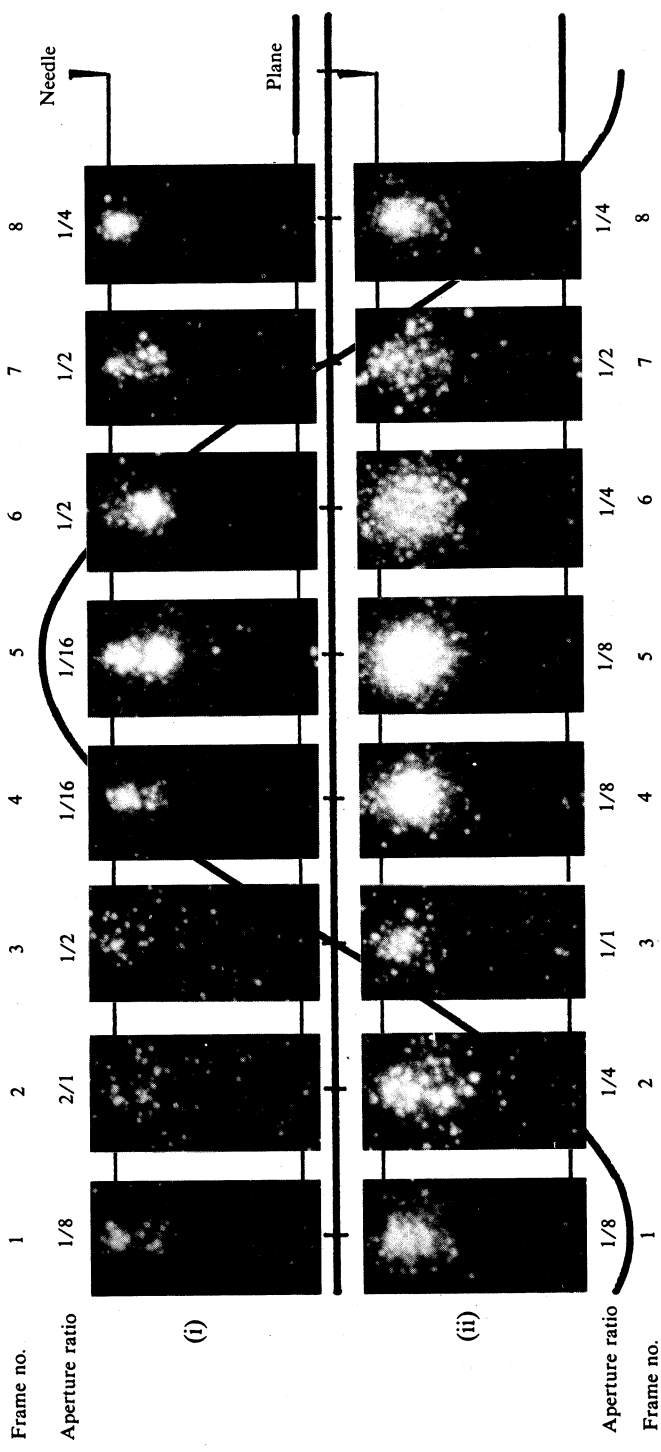

Fig. 5. Variation of the corona image at 200 Torr in air taken with a u.v. filter at (i) $T = 0{\cdot}9$ μs and $V_p = 2550$ V; (ii) 5 μs and $V_p = 4200$ V.

irregular filaments extending out from the enlarged corona boundary surface and these culminate in further intermittent discharges. By contrast, as seen in Fig. 2*b*, there is a continuous progression in the growth of the corona around a negative needle point and intermittent discharge events are not observed.

At 650 Torr the stabilised corona discharge could not be observed after the initiation of the intermittent breakdown. At these pressures the intermittent events developed directly into the continuous breakdown phase which accounts for the lower values of V_{sc} observed at $pd = 780$ Torr cm in Fig. 1*a*.

Explanations for the differences between V_c versus pd_c in air and N_2 and for the differences with intermittent discharges in these two gases are most likely to be associated with the space-charge quenching of the discharge observed also with d.c. corona in electronegative gases (Farish *et al.* 1978). This is discussed more fully in Section 3.

(b) Development of the Corona Discharge at 200 Torr

Ten-nanosecond snapshot photographs of the corona discharge in air at 200 Torr are shown in Figs 3(i) to 3(iv). They were taken at various phase positions within a single cycle of the applied r.f. voltage and at different stages T of the 10 μs pulse. Multi-exposed photographs taken under conditions similar to those in Figs 3(ii) and 3(iv) are shown in Figs 4(i) and 4(ii) respectively. In all these cases the peak applied r.f. voltage $(V_p)_{max}$ was 4200 V.

As in the case of N_2, it is the radiation from the second positive system of the nitrogen molecules that gives rise to the corona images in air. However, in air the effective lifetime associated with these excited states is small enough to ensure that any contribution to the image at one phase position by the radiation persisting from the earlier phase position can be ignored.

The following significant features of the corona images should be noted:

(1) Although the corona images in air are less intense and not so extensive as those in nitrogen, nevertheless the same polarity and hysteresis effects are observed.

(2) The development of the corona at the positive needle shows similarities with the characteristic Type A, B and C images observed in nitrogen. For example:—

  (a) At $T = 0{\cdot}75$ μs, just after the corona initiation [Fig. 3(i)] the corona discharge is localised around the needle tip (Type A image).

  (b) At $T = 0{\cdot}9$ and $1{\cdot}0$ μs [Figs 3(ii) and 4(i)], the discharge has 'stepped' away from the surface of the brightly luminous region toward the plane electrode, leaving the corona of the earlier time anchored to the needle tip. This ellipsoid-shaped image was identified as Type B in the nitrogen observations.

  (c) At $T = 1{\cdot}4$ μs this extended corona is suppressed whilst at the same time the corona anchored at the needle point expands in the radial direction at both the positive and succeeding off-peak phase position [Fig. 3(iii)]. Whilst such an image was not observed in N_2, it bears some resemblance to the pear shape identified in N_2 as Type C.

  (d) With further increase in T to 5 μs [Figs 3(iv) and 4(ii)], the corona discharge expands to spherical form, which we now call Type D, over the region from needle tip to mid-gap. When the peak applied voltage

$(V_p)_{max}$ was lowered, image types B and C appeared at the larger values of T, but Type D did not appear at all. Table 1 summarises the time intervals associated with the appearance of the various types of images.

Figs 5(i) and (ii) show the effects of using a u.v. filter ($\lambda_{cutoff} < 390$ nm) and can be compared with Figs 3(ii) and (iv). In contrast to the observations in nitrogen there is little or no change in the appearance of the corona images when the u.v. filter is used, although the intensity of the corona image decreases to some 50% of that observed without the u.v. filter.

Table 1. Time delays T (μs) for the appearance of various types of images at three values of the peak voltage (V)

$(V_p)_{max}$	Corona onset	A	B	C	D
3000	$T = 1$	1·0 ~ 1·1	1·1 ~ 1·75	1·75 ~ 8	
	$V_p = 1950$	1950 ~ 2100	2100 ~ 2700	2700 ~ 3000	
3600	$T = 0·8$	0·8 ~ 0·9	0·9 ~ 1·5	1·5 ~ 8	
	$V_p = 2100$	2100 ~ 2400	2400 ~ 3000	3000 ~ 3600	
4200	$T = 0·7$	0·7 ~ 0·8	0·8 ~ 1·4	1·4 ~ 3	3 ~ 8
	$V_p = 2100$	2100 ~ 2250	2250 ~ 3150	3150 ~ 4050	4050 ~ 4200

(c) Development of the Corona Discharge at 80 and 650 Torr

In general, the corona images appearing in air and N_2 at low pressure resemble each other more closely than the corresponding images at higher pressure.

Figs 6(i) and (ii) show the multi-exposed photographs at 80 Torr. The discharges are more diffuse at these lower pressures. They do not, however, extend as far in the direction of the plane electrode as do those in N_2. Evidence of the 'stepped' progress of the corona is present at $T = 1·2$ μs but the pear-shaped Type C corona image does not appear at this lower pressure. As was the case in nitrogen, localised luminosity can be seen in the neighbourhood of the plane electrode at both the off-peak and zero positions following the negative peak voltage.

At the higher pressure of 650 Torr, significant differences between the corona discharges in air and nitrogen were observed. For $(V_p)_{max} = V_p = 3300$ V the corona discharge is confined to a small region in the neighbourhood of the needle tip at the early times T. Under the same conditions at $T = 8$ μs the corona discharge extends irregularly towards the plane electrode [Fig. 7(i)] without significant expansion laterally. When one of the extended filaments reaches the plane electrode intermittent breakdown is achieved. With increasing $(V_p)_{max}$ and V_p the forked filaments show up very clearly as seen for $(V_p)_{max} = V_p = 5100$ V in Fig. 7(ii). The mechanism responsible for the transition from such corona discharges to spark breakdown in air at $pd = 650$ Torr cm appears to be quite different from that operating at lower pressures and leads to the remarkable decrease of V_{sc} at this pressure (see Fig. 1*a*).

(d) Spectroscopic Observations of the Corona Discharge in Air

The variation of intensity of some typical spectral emission observed with a spatial resolution of 0·2 mm in the region between the needle-point and mid-gap is shown in Fig. 8. The spatial variation of the spectral emission intensity can be seen as an envelope of spikes of individual tracks, each of which contains information on spectral emission. The information selected is that for the (*a*) negative peak and (*b*) positive

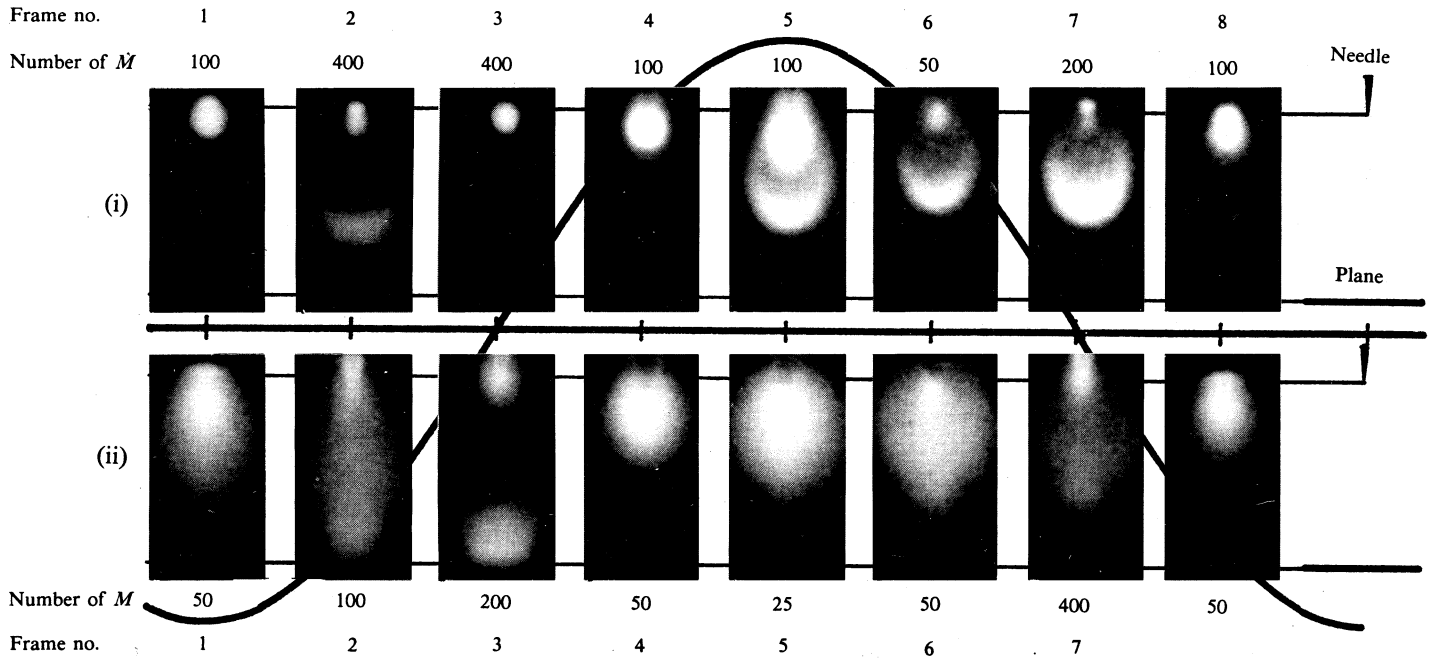

Fig. 6. Variation of the corona image at 80 Torr in air taken with two-stage MCP image intensification and multi-exposures at (i) $T = 1{\cdot}2\ \mu s$ and $V_p = 1950$ V; (ii) $T = 5\ \mu s$ and $V_p = 2400$ V.

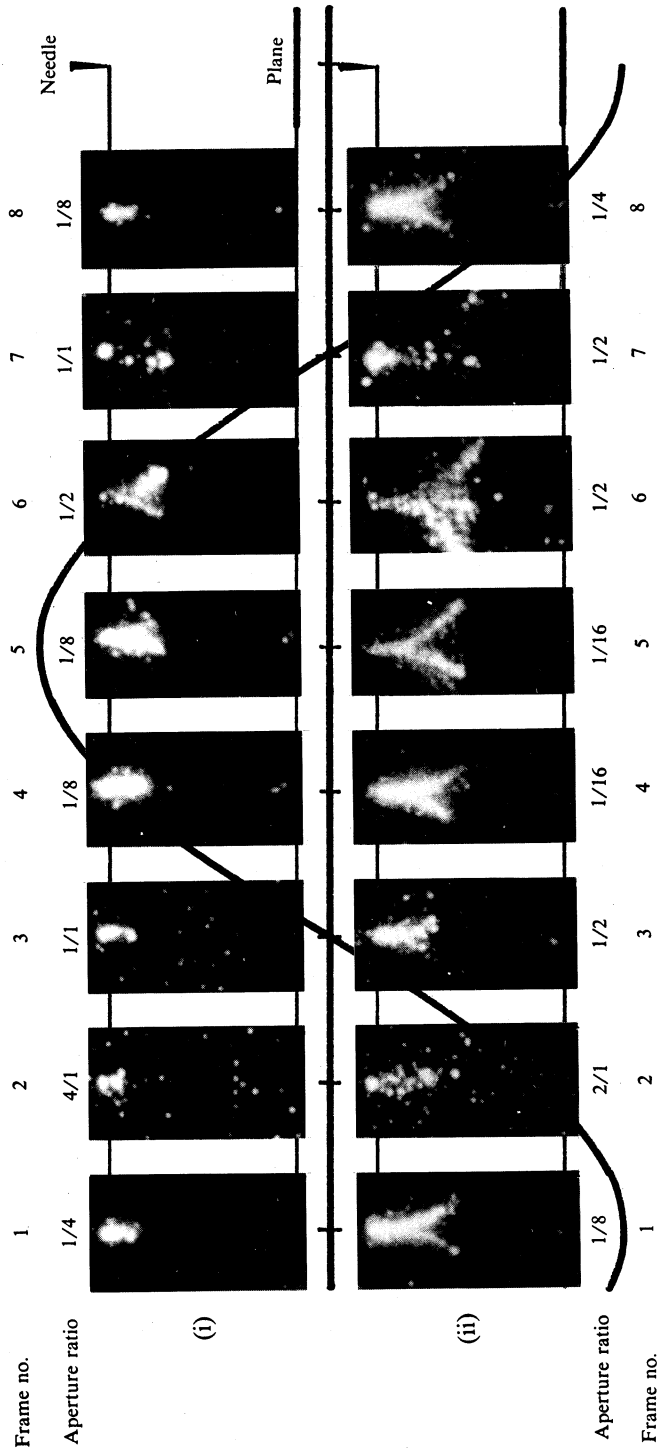

Fig. 7. Variation of the corona image at 650 Torr in air at (i) $T = 8\ \mu s$ and $V_p = 3300$ V; (ii) $T = 8\ \mu s$ and $V_p = 5100$ V.

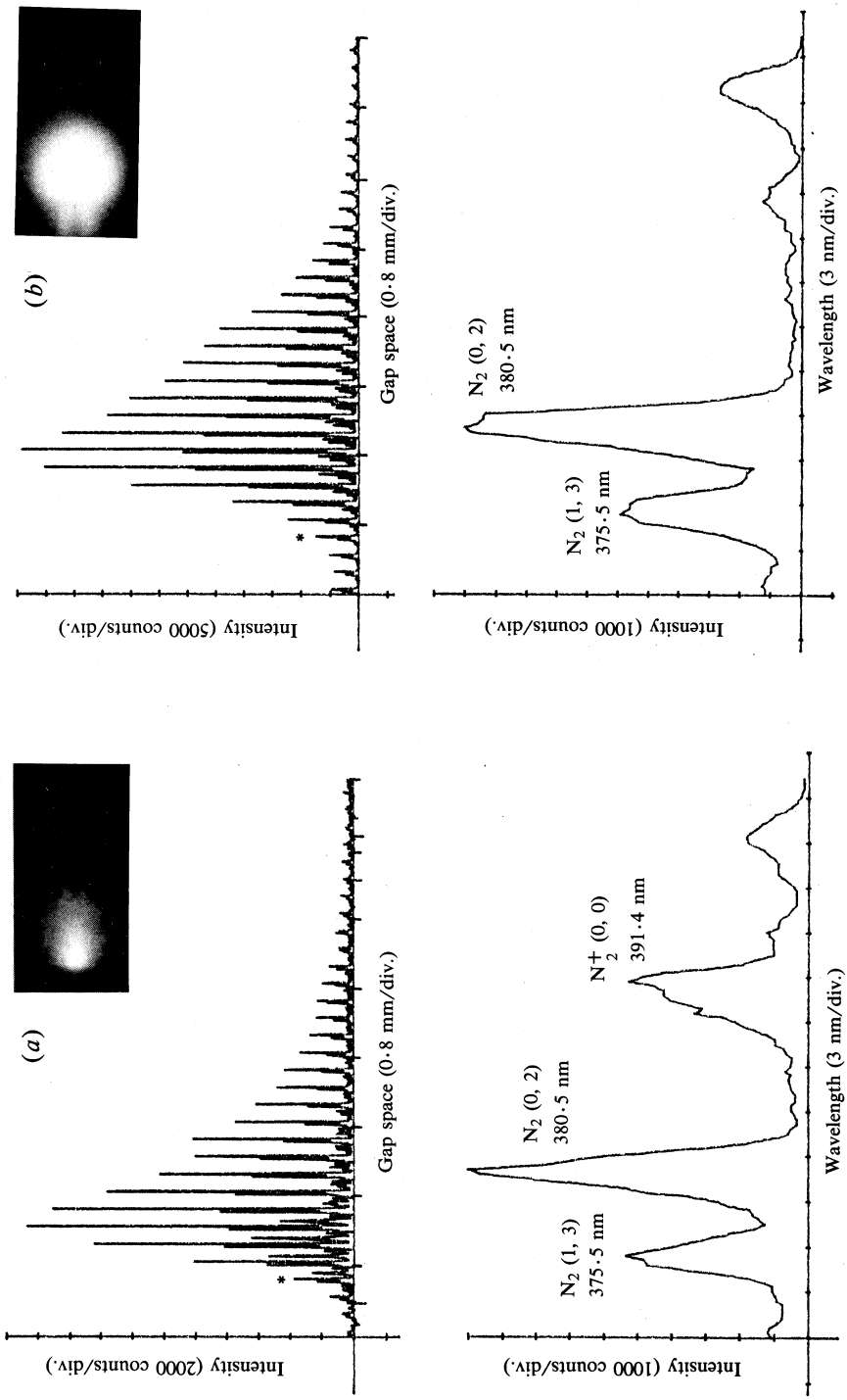

Fig. 8. Spectral emissions at $T = 5$ μs and $p = 200$ Torr in air for (*a*) the negative peak and (*b*) the positive peak. The fourth track, marked by an asterisk, corresponds to the position of the needle tip.

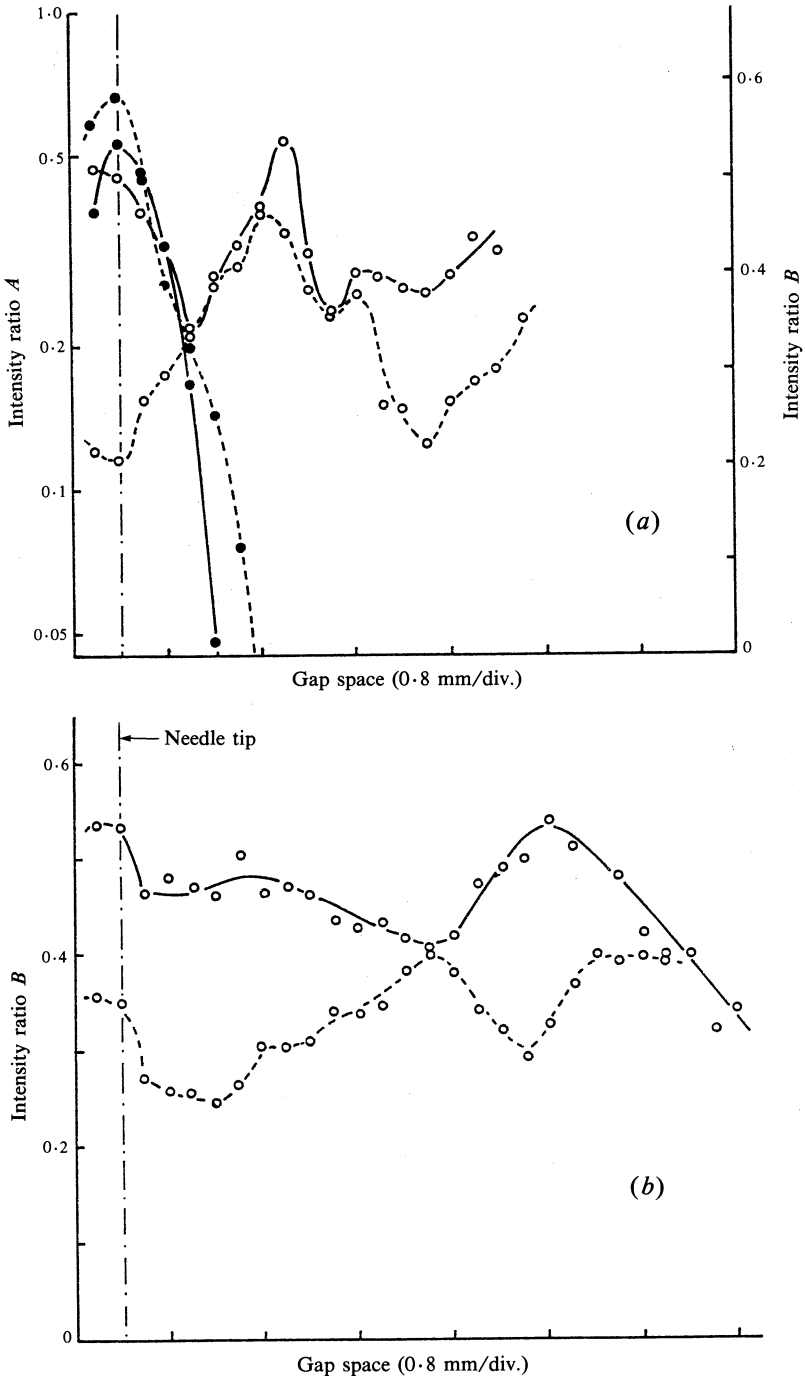

Fig. 9. Spatial variation of the intensity ratios A (solid circles) and B (open circles) at $T = 5$ μs in air (solid curves) and nitrogen (dashed curves) at 200 Torr at (*a*) the negative peak and (*b*) the positive peak.

peak phase positions at $p = 200$ Torr. Also shown are the spectra corresponding to a particular track (indicated by an asterisk in Fig. 8) in the neighbourhood of the positive and negative needle electrode. From these observed spectral lines, the spatial variation of the intensity ratios of $I_{N_2^+}(0,0)$ and $I_{N_2}(1,3)$ to $I_{N_2}(0,2)$ can be obtained. Furthermore, it is also possible to establish the temporal variations of such ratios during one single cycle of the applied r.f. voltage at any time T. These spatio-temporal variations of the intensity ratios in air are essentially the same as those observed in nitrogen and show the same polarity effect, hysteresis and progressive changes with T. Consequently, in the following, we concentrate only on the differences between the spectra in air and nitrogen.

The spatial variations of the two intensity ratios measured in air and nitrogen at 200 Torr are compared, for negative and positive peak phase positions, in Figs 9*a* and 9*b*. In both air and nitrogen it is only possible to measure the intensity ratio $I_{N_2^+}(0,0)/I_{N_2}(0,2)$ (ratio A) in the neighbourhood of the needle tip at negative polarity. The ratio decreases sharply with increasing distance from the needle tip, decreasing more rapidly in air than in nitrogen. The maximum value of the ratio A in air at the needle tip is also smaller than that in nitrogen.

The intensity ratio $I_{N_2}(1,3)/I_{N_2}(0,2)$ (ratio B) can be measured at both peak negative and peak positive needle voltage. In air, at peak negative, it decreases with increasing distance from the needle tip and a minimum value occurs at a distance of about 1·2 mm. By contrast the minimum value of B in nitrogen occurs at the needle tip and is smaller than the value in air. Perhaps the most significant feature of the observations is that the values of B measured in air at both peak negative and peak positive are considerably larger than those in nitrogen.

(e) Theoretical Consideration of the Spectral Intensity Ratio

The values of the intensity ratios A and B depend on the mean electron energy, the electron energy distribution function and the optical electron excitation cross section. They are also sensitive to the particular quenching processes affecting the excited molecules responsible for the specific spectral emissions. The quenching factor is defined as the percentage of the total radiative, electronic and vibrational deactivations attributable to the radiative deactivations of the specific level. In particular, the presence of oxygen molecules strongly influences the quenching factors Φ^{C}_{q0}, Φ^{C}_{q1} and Φ^{B}_{q0} of the corresponding excited levels of nitrogen $C\,^3\Pi_u(v' = 0)$, $C\,^3\Pi_u(v' = 1)$ and of N_2^+ $B\,^2\Sigma_u^+(v' = 0)$ through such reactions as (Gallimberti *et al.* 1974)

$$N_2(C\,^3\Pi_u)_{v'} + O_2(X\,^3\Sigma_g^-)_{v'=0} \rightarrow NO(X\,^2\Pi)_{v''} + NO(A\,^2\Sigma^+)_{v''\geqslant 0},$$

and similar reactions for the N_2^+ $(B\,^2\Sigma_u^+)$ state.

Table 2 shows the values of the quenching factors at 200 Torr in air and nitrogen, calculated by using the specific deactivation processes, including the cascade process, proposed by Gallimberti *et al.* For comparison with previous experimental data (Sato and Haydon 1986*b*), in the calculations we have assumed the nitrogen sample contains 0·5% oxygen contamination.

It can be seen that the rapid deactivation of the $C\,^3\Pi_u$ levels by oxygen leads to larger values of the ratios $\Phi^{C}_{q1}/\Phi^{C}_{q0}$ and $\Phi^{B}_{q0}/\Phi^{C}_{q0}$ for air than for nitrogen, these ratios in turn being directly proportional to the values of the intensity ratios. Calculation of

Table 2. Quenching factors at 200 Torr in air and N_2 with 0·5% oxygen

Quenching factor	Air	N_2
$N_2\,C\,^3\Pi_u(v'=0)$; Φ^C_{q0}	0·039	0·124
$N_2\,C\,^3\Pi_u(v'=1)$; Φ^C_{q1}	0·049	0·226
$N_2^+\,B\,^2\Sigma_u^+(v'=0)$; Φ^B_{q0}	0·0047	0·0052
Φ^C_{q1}/Φ^C_{q0}	0·796	0·549
Φ^B_{q0}/Φ^C_{q0}	0·121	0·042

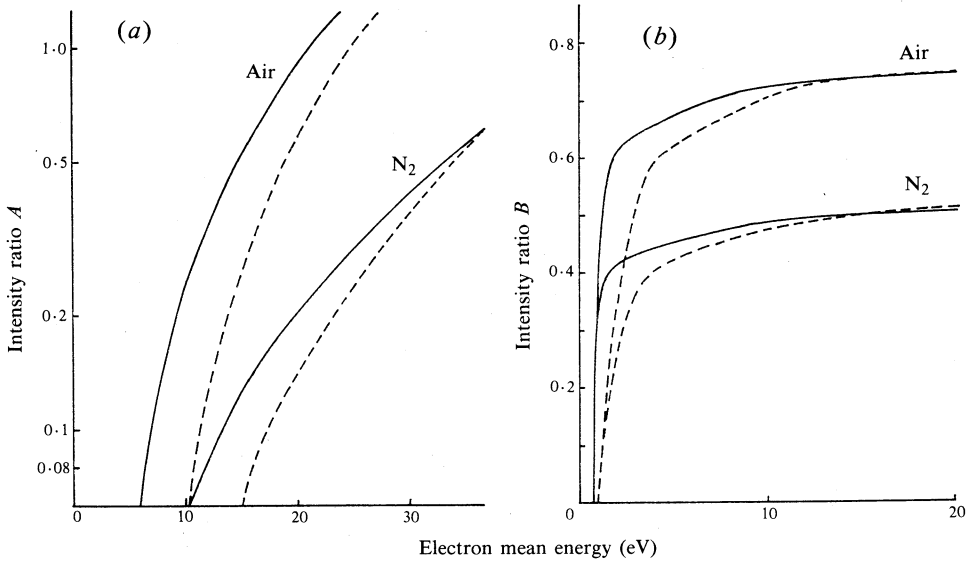

Fig. 10. Variation of the (*a*) intensity ratio *A* and (*b*) intensity ratio *B* with electron mean energy, assuming Maxwellian (solid curves) or Druyvesteyn (dashed curves) distribution functions in air and nitrogen with 0·5% oxygen contamination at 200 Torr.

Table 3. Comparison of observed intensity ratios and estimated electron mean energies for air and N_2 + 0·5% O_2 based on assumed Maxwell (M) and Druyvesteyn (D) distribution functions

Negative needle tip					Positive needle tip					
Ratio $(A)_{max}$		$\bar{\epsilon}$ (eV)			Ratio *B*		$\bar{\epsilon}$ (eV)			
Air	N_2	Air	Air	N_2	Air	N_2	Air	N_2	Air	N_2
0·52	0·64	15	19	40	0·3–0·5	0·25–0·4	2–3	2–4	0·8–1·2	0·8–1·5
Assumed distribution function		M	D	M & D			D	D	M	M

the ratios *A* and *B* requires knowledge of the appropriate electron energy distribution functions and optical electron excitation cross section. The procedure outlined in the earlier paper for N_2 (Sato and Haydon 1986*b*) has also been followed for air in which either a Maxwellian or Druyvesteyn distribution function is assumed. The calculations, summarised in Figs 10*a* and 10*b*, confirm that both ratios *A* and *B* are larger in air than in nitrogen due essentially to the larger ratios of the quenching factors in air.

plane electrode will an intermittent breakdown event be recorded. Eventually the corona discharge stabilises again at some higher voltage with a corresponding larger volume of ionised gas (corona). The process repeats itself in much the same way as the 'stepped' leader phenomena associated with the early stage of the development of the lightning discharge. Ultimately a spark discharge develops. At atmospheric pressure the instabilities leading to filamentary processes become so strong that the transition to continuous spark breakdown takes place without the need for a sequence of intermediate corona stabilisations; V_{sc} is then $\sim V_i$.

For the case of a d.c. corona, stabilised discharges have been observed only at pressures greater than one atmosphere in gases such as SF_6 and air (Farish *et al.* 1978; Malik and Qureshi 1979). In the present r.f. experiments stabilised corona could be observed at pressures less than one atmosphere, which indicates that higher densities of negative and positive ions than under d.c. conditions can be accumulated in this case.

Finally, some comments should be made about the development and associated suppression of the corona discharges in air at pressures of $\sim$80 to 200 Torr. Spectroscopic observations have indicated (Table 3), that the electron mean energies in air are lower than those in nitrogen, both in the neighbourhood of the needle-point and in mid-gap. This is to be expected if electron attachment processes play an important role. Furthermore, it is consistent with the following considerations of the consequences of space-charge accumulations on the electric field distributions.

In the case of N_2 positive space charge accumulated in the high field region in front of the needle electrode and at peak positive voltage caused the electric field to decrease in the region between the needle tip and the positive space charge, so creating a moderate peak in the electric field at mid-gap. In air the effects of electron attachment lead to some significant differences. For example, negative ions now accumulate in the low field region produced by the positive space charge in front of the needle electrode, as well as between mid-gap and the plane electrode. At peak positive voltage, both the field in front of the needle tip as well as the peak field in mid-gap are increased, whereas the field between mid-gap and plane electrode is decreased. The loss of electron density in the low field regions means that luminescence is now observed only in the high field region in front of the needle tip and at mid-gap. A dark strip appears between these two high field regions. Therefore, as a consequence of electron attachments, there is a 'stepped' appearance to the corona image. Furthermore, the same processes lead to the build up of negative ion space charge in the region between mid-gap and plane electrode and at peak positive voltage cause a decrease in the electric field in this region. This inhibits any further extension of the corona discharge, which is then suppressed.

There is clearly a need for further precise analysis, using appropriate computer simulation and taking the electron attachment effect into account, before we can establish more precisely how the corona discharge mechanism develops in air.

Acknowledgments

The authors wish to acknowledge the continued support provided by the Electrical Research Board for this project. Further help with instrumentation has been given by the Australian Institute for Nuclear Science and Engineering and more recently by the Australian Research Grants Committee. The authors also wish to acknowledge the help of T. Kamibayashi in preparing the photographs for publication.

References

Farish, O., Ibrahim, O. E., and Korasli, C. (1978). Fifth Int. Conf. on Gas Discharges, Liverpool, pp. 320–3 (IEE: London).
Gallimberti, I., Hepworth, J. K., and Klewe, R. C. (1974). *J. Phys.* D **7**, 880–98.
Kücükarpaci, H. N., and Lucas, J. (1979). *J. Phys.* D **12**, 2123–36.
Malik, N. H., and Qureshi, A. H. (1979). *IEEE Trans. Electr. Insul.* **EL-14**, 1–13.
Sato, N., and Haydon, S. C. (1984*a*). *J. Phys.* D **17**, 2009–21.
Sato, N., and Haydon, S. C. (1984*b*). *J. Phys.* D **17**, 2023–36.
Sato, N., and Haydon, S. C. (1986*a*). *Aust. J. Phys.* **39**, 271–91.
Sato, N., and Haydon, S. C. (1986*b*). *Aust. J. Phys.* **39**, 293–307.
Sato, N., and Tagashira, H. (1985). *J. Phys.* D **18**, 2451–61.
Taniguchi, T., Tagashira, H., and Sakai, Y. (1978). *J. Phys.* D **11**, 1757–68.

Manuscript received 27 November 1986, accepted 3 April 1987